Biomass pyrolysis devolatilization kinetics of herbaceous and woody feedstocks

Chad A. Peterson[1], Malachi K. Hornbuckle[2], Robert C. Brown [1,2]

[1]*Department of Mechanical Engineering, Iowa State University, Ames, IA 50011, United States*

[2]*Bioeconomy Institute, Iowa State University, Ames, IA 50011, United States*

Corresponding author's e-mail address: rcbrown3@iastate.edu

Highlights

- Devolatilization kinetics were determined for four biomass feedstocks.
- A single global rate accurately modeled formation of pyrolytic vapours.
- Apparent devolatilization activation energies were in the range of 54.9-88.4 kJ mol^{-1}.
- Biomass inorganic content did not affect devolatilization rates.

Abstract

Devolatilization kinetics were determined using a modified micropyrolyzer reactor for several biomass feedstocks: switchgrass, corn stover, red oak, and pine. The micropyrolyzer was directly coupled to a flame ionization detector (FID) to track the release of volatiles from the biomass. Time series data from these experiments was analysed to determine apparent devolatilization rates. Care was taken to assure the experiments were isothermal and kinetically limited calculating a Biot number less than 0.1 and pyrolysis numbers greater than 10, which simplifies the derivation of devolatilization rates. A single, first order reaction was able to model devolatilization rates at temperatures up to 500°C. No correlation was found between the inorganic content of the biomass and its rate of devolatilization. Apparent activation energies were in the range of 54.9-88.4 kJ mol^{-1}. The calculated rate coefficient at 500°C was calculated as 1.90-5.14 s^{-1} for the four feedstocks.

Keywords

Pyrolysis, biomass, devolatilization rate, chemical kinetics

1. Introduction

In a matter of seconds, fast pyrolysis devolatilizes solid biomass into condensable vapors (bio-oil) and non-condensable gases (NCG) leaving a solid residue (biochar) [1]. Many researchers have investigated the rate of devolatilization, but results show large variations. Accurate kinetic data is important to the design of fast pyrolysis systems.

Biomass devolatilization rates have been measured for a variety of feedstocks (e.g., pine, cellulose, switchgrass) using several kinds of experimental methods (TGA, fluidized beds, screen heaters) [2,3]. Measurement of mass changes, composition of liquid products, and gas yields are commonly used to derive devolatilization rates [3]. These diverse approaches have yielded inconsistent devolatilization kinetics (Table 1). Even when different groups use similar methodologies, differences arise from inconsistencies in heating rates, final temperatures, and particle sizes employed in the experiments. Rapid heating rates (>100°C s^{-1}) and elevated final temperatures (500°C) are crucial for deriving chemical kinetic data relevant to fast pyrolysis of biomass. Unfortunately, many commonly cited devolatilization models (as discussed below) do not adhere to these criteria when measuring reaction kinetics.

Miller and Bellan [4] developed a devolatilization model for the individual bio-polymers of hemicellulose, cellulose, and lignin. This model employed cellulose devolatilization kinetics attributed to Blasi et al.[5], but actually originate from the earlier work of Bradbury et al [6]. Bradbury et al.[6] limited their study to the temperature range of 259-341°C, much lower than typical fast pyrolysis temperatures (400-500°C). Similarly, a one-step global devolatilization model developed by Blasi et al.[7] used thermogravimetric analysis (TGA) data obtained in the

temperature range of 300-435°C. TGA experiments, while allowing for accurate measurement of mass changes with time, cannot achieve the high heating rates characteristic of fast pyrolysis of biomass. Blasi et al.[7] employed a heating rate of only 16°C s^{-1}, an order of magnitude slower than typical of fast pyrolysis (~100°C s^{-1}). The relatively large mass of the sample cups (often greater than 100 mg) used in TGA experiments is responsible for this slower heating rate. At these slow heating rates and low temperatures, dehydration and carbonization reactions are more prominent than typical of fast pyrolysis [8]. Notably, bio-oil yields are higher at rapid heating rates (>100°C s^{-1}) compared to slow heating rates (<10°C s^{-1}) [9]. Consequently, this data, although commonly employed in computational models of fast pyrolysis [10][11], have limited utility for modeling fast pyrolysis.

Measuring devolatilization kinetics at temperatures characteristic of fast pyrolysis (400-500°C) is critical for determining relevant kinetics. Unfortunately, even studies performed at elevated temperatures (>400°C), often have deficiencies. Sadhukhan et al. [12] used a screen heater to pyrolyze 350-500μm diameter wood particles, calculating a suspiciously low apparent activation energy for devolatilization of 51.6 kJ mol^{-1}. While the temperatures employed (250-600°C) were relevant to fast pyrolysis, the experimental conditions are otherwise problematic. Despite claiming isothermal conditions, important for accurate kinetic measurements, their measurements of internal particle temperature indicated times on the order of minutes were required to reach the reported reaction temperature. To avoid these types of errors, calculation of particle Biot number is paramount in confirming particle heating is fast enough for devolatilization to occur under essentially isothermal conditions.

Wagenaar et al. [13], whose work is frequently mistakenly attributed to Janse et al. [14], attempted to minimize internal temperature gradients by hammer milling pine particles to a 100-

212 μm diameter. The model assumed a one-step parallel reaction for the non-condensable gases (NCG), biochar, and tar (bio-oil) from particle mass loss. Both TGA experiments at reaction temperatures up to 400°C and drop tube furnace experiments with furnace temperatures between 500-600°C were conducted. While the drop tube experiments were conducted at temperatures relevant to fast pyrolysis, their reported reaction rates are suspiciously high, possibly arising from inadequate quenching of reaction after the desired reaction time. In their drop tube experiments, Wagenaar et al. [13] used "cold equimolar nitrogen" (temperature unknown) to quench reactions after passage of particles through the reactor. The reported solids conversion at 550°C were as high as 75% for a residence time in the heated section of the drop tube of 0.45 s. In contrast, Gable and Brown [15], using a free-fall reactor of similar design to Wagenaar et al. [13] but employing large quantities of very cold (-178°C) nitrogen to quench reaction, measured much lower solids conversion of around 40% at 550°C for a residence time of 1.5 s. Gable and Brown [15] cautioned that inadequate quenching after passage through the reaction zone could result in particles "smoldering" for much longer than the reactor residence time, resulting in significant inaccuracies in measurement of reaction rate.

Although not discussed, Wagenaar et al. [13] measured notable differences in biomass reactivity for their TGA and drop tube experiments with measured activation energies of 150 kJ mol^{-1} and 110 kJ mol^{-1}, respectively. This notable difference suggests that the lower temperatures and slower heating rates in a TGA introduces large errors in estimating rates of fast pyrolysis.

Liden et al. [16] used product yields (bio-oil, biochar, and NCG) from a fluidized bed reactor to develop a devolatilization model for pyrolysis. By varying the reactor temperature and gas vapor residence time, a parallel-step model of pyrolysis was developed. The paper has been widely cited as a source of pyrolysis kinetic data since it was published in 1988 despite the authors'

caution that the results should be viewed as preliminary since insufficient data was collected to fully validate the model.

Other studies have similarly measured the yield of volatile products to determine devolatilization kinetics. For example, Pielsticker et al. [17] used a fluidized bed reactor in conjunction with an online FTIR gas analyzer to derive the devolatilization rate of beech wood at temperatures between 350 and 700°C. The activation energy for pyrolysis was estimated to be 71.3 kJ mol^{-1}. However, the model assumed isothermal particles, although neither measurements nor calculations were employed to confirm this assumption. The 125-160 μm particles were likely large enough to result in small temperature gradients through the particles, skewing the calculation of reaction rates. Under the rapid heating of fast pyrolysis, particles must generally be smaller than 100 μm to avoid internal temperature gradients [18]. Even small deviations from isothermal reaction can noticeably affect measured rates.

Even when efforts are made to account for particle heating rates determining pyrolysis rates from non-isothermal experiments can be problematic. Zolghadr et al. [19] used a novel micro-reactor with rapid particle heating (>1000°C/s) to determine devolatilization kinetics. A “fast response” FID was able to provide time series data with millisecond resolution. Devolatilization times were about 2 s for pyrolysis of cellulose and switchgrass at 500°C. Most measurements were made at temperatures much higher that typical of fast pyrolysis (up to 900°C). A follow-up publication determined the activation energy for devolatilization of 92 μm switchgrass particles at 500°C to be 167.3 kJ mol^{-1} [20]. However, the apparent activation energy varied by ~50 kJ mol^{-1} for experiments at different temperatures and particle diameters. Given direct temperature measurements were not possible, the authors calculated model parameters (temperature, reaction rate, heat of reaction, etc.) simultaneously estimating particle temperature from the measured

FID signal and particle injection time. Accordingly, any erroneous assumptions in calculating particle temperature from the heat transfer model, which was not validated, would propagate to inaccurate calculations with the reaction rates.

Recent advances in computational modeling of the thermal behavior of biopolymers have improved the understanding of pyrolysis kinetics. Vinu and Broadbelt [21] used density functional theory (DFT) to develop a mechanistic model for cellulose depolymerization. The activation barriers for the polymer (analogous to bond strength) were calculated as 49.5 kcal mol^{-1} for chain initiation and 51.5 kcal mol^{-1} for end-chain initiation. The model was compared to experimental data obtained from micropyrolysis of cellulose at 500°C. However, only product yields were used to validate the model since conventional micropyrolysis experiments do not yield rate data. Broadbelt's group also developed a pyrolysis mechanism for hemicellulose (using xylose as a proxy). They predicted activation energies of 53.5 kcal mol^{-1} for initiation and 51.5 kcal mol^{-1} for end-chain initiation, similar to cellulose [22]. Comparison with data from micropyrolysis of xylose at 500°C found agreement with predicted product yields.

The mechanistic models suggest that reaction times for pyrolysis of cellulose and hemicellulose at 500°C are 2 s and 4.5 s, respectively, which is comparable to the time scale for biomass devolatilization measured experimentally [23]. However, the large activation energies determined from DFT modeling (>150 kJ mol^{-1}) predict reaction times increasing to hundreds of seconds as pyrolysis temperature decreases to 400°C [24] while actual pyrolysis time is two orders of magnitude shorter [25].

Table 1 Examples of commonly used global models for biomass pyrolysis. The models capture devolatilization rates and exclude subsequent vapor cracking reactions. For a given temperature, reaction rates calculated from these models can disagree by as much as an order of magnitude.

							Global Bio-oil rate coefficient (s^{-1})		
Model	**Activation Energy (kJ mol^{-1})**	**Pre-Exponential (s^{-1})**	**Feedstock**	**Reactor**	**Method**	**Temperature (°C)**	**400 °C**	**500 °C**	**600 °C**
Blasi et al.[7] (2002)	148.8	1.08×10^{10}	Beech Wood	TGA	Solid Mass Loss	300-435	3.04×10^{-2}	9.48×10^{-1}	1.34×10^{1}
Wagenaar et al.[13] (1994)	150.0	1.40×10^{10}	Pine Wood	TGA + Drop Tube	Solid Mass Loss	300-600	3.19×10^{-2}	1.02×10^{0}	1.48×10^{1}
Sadhukhan et al.[12] (2008)	52.0	1.68×10^{2}	Wood	Tube Reactor	Solid Mass Loss	250-600	1.56×10^{-2}	5.18×10^{-2}	1.31×10^{-1}
Liden et al.[16] (1988)	183.3	1.00×10^{13}	Wood	Fluidized Bed	Pyrolysis Yields	450-600	5.93×10^{-2}	4.10×10^{0}	1.08×10^{2}
Pielsticker et al.[17] (2019)	71.4	3.26×10^{4}	Beech Wood	Fluidized Bed	Gas volatiles	350-700	9.31×10^{-2}	4.86×10^{-1}	1.73×10^{1}
Zolghadr et al.[20] (2019)	167.3	2.52×10^{12}	Switchgrass	Microreactor	Gas volatiles	500-900	2.60×10^{-1}	1.25×10^{1}	2.46×10^{2}

Alkali and alkaline earth metals (AAEM) are well known to catalytically crack pyranose rings into light oxygenated components [26,27]. Even at low concentrations (<1 wt.%) these metals can significantly reduce the yield of anhydrosugars. While it is well known these metals can impact product yield, their impact on the devolatilization rate is less well established. In particular, some researchers have found impregnating whole biomass with these metals (i.e., potassium) can increase devolatilization rate and reduce overall activation energy [28,29]. Conversely, Johansen et. al.[30] reported that metal content did not significantly affect devolatilization rate. While these previous inconclusive results were experimental in nature, computational (mechanistic) modeling efforts are also inconclusive. For their computational model of glucose pyrolysis, Mayes et al.[31] determined that sodium increased the rates by an average of 5.9. However, the standard deviation was 14, indicating that some pathways were slower as a result of adding sodium. These conflicting results complicate modeling efforts as biomass composition can vary among woody and herbaceous feedstocks.

The goal of this work is to explore devolatilization rates under fast pyrolysis conditions using experimental methods that overcome limitations of previous experimental and computational studies. Utilizing a modified micropyrolyzer, we collected time-series data on the evolution of volatiles from fast pyrolysis of several kinds of biomass. The diversity of AAEM content among the biomass samples allowed us to investigate the effect of AAEM content on devolatilization kinetics.

2. Methods

2.1. Feedstock characterization

Four biomass feedstocks were used in these experiments: red oak, corn stover, switchgrass, and pine. These are representative of herbaceous and woody biomass commonly used as feedstocks in fast pyrolysis [32,33]. To provide a homogeneous sample, feedstocks were ball milled to an average of 60 μm size. Proximate analysis indicated the herbaceous materials contained significantly more inorganic content (ash) than the woody feedstocks (Table 2).

Table 2 Proximate Analysis of the four feedstocks used in these experiments.

	Biomass Basis wt.% (as received)			
	Switchgrass	**Corn Stover**	**Red oak**	**Pine**
Moisture	6.7	6.0	5.0	6.0
Volatile Content	76.1	73.0	82.2	80.4
Fixed Carbon	12.2	11.0	10.1	10.9
Ash	4.9	10.0	2.8	2.7

Inductively coupled plasma (ICP)-Optical Emission Spectrometry (OES) provided partial elemental analysis of the feedstocks shown in Table 3. For the procedure, the samples were digested in nitric acid via microwave heating. The samples were then diluted 10,000-fold with 18.2 Ω water. Quantification followed standard acid digestion method ASTM D6349. Notably, the herbaceous feedstocks contained significantly higher quantities of potassium and calcium as compared to the woody feedstocks.

Table 3 Minor compositional analysis of the biomass feedstock from ICP. Herbaceous feedstocks contained significantly greater concentration of AAEM as compared to herbaceous material.

	Biomass Inorganic Content (parts per million-PPM)			
	Switchgrass	**Corn Stover**	**Red oak**	**Pine**
Aluminum	91	1,370	26	21
Calcium	2,616	3,631	1,795	557
Copper	-	-	-	-
Iron	113	1,104	15	23
Magnesium	1,432	1,912	153	151
Manganese	94	83	29	34
Phosphorus	508	350	23	48

Zinc	6	9	-	5
Sodium	198	239	40	37
Potassium	4,178	6,564	1,081	613

2.2. Micropyrolysis experiments

Pyrolysis experiments were conducted with a modified Frontier micropyrolyzer (PY-2020, Frontier Laboratories, Japan) in combination with a modified GC-FID. Bruker 430 GC-FID A small hook originally designed to suspend sample cups in the microreactor was employed to directly adhere powdered biomass via weak Coulomb forces (see Fig. 1). Although the mass of particles on the hook was not measured, visual inspection suggested that samples weighed less than 1 mg. This quantity was small enough to avoid heat and mass transfer limitations during the test, assuring that chemical kinetics were being measured. The furnace section of the micropyrolyzer was modified to include three screens to intercept biomass particles injected in the furnace and rapidly heat them. The heated screens consisted of a 250 μm copper screen between two 316 stainless steel screens of 90 μm mesh. Given the large mass of the screens (>100 mg) compared to the 0.1 mg mass of biomass samples that impinged on them during experiments, they were expected to remain isothermal during experiments. The interface between the micropyrolyzer and the GC (Bruker) was maintained at 400°C. Rather than a standard GC column, a 0.50 m long high temperature Agilent deactivated GC column was employed in the GC (also operated at 400°C) with a gas-split ratio of 250:1, which achieved rapid transport of pyrolysis vapors from the micropyrolyzer to a Bruker 430 GC-FID, thus minimizing instrument lag time.

For each test, a biomass-loaded sample hook was installed in the micropyrolyzer in the cool region above the furnace zone (see Fig. 1). The micropyrolyzer furnace was brought to the

desired reaction temperature with helium flow rate of 250 mL min^{-1}. At this point, the helium flow was manually interrupted by closing the supply valve for three seconds. By rapidly reopening the valve, the sudden rush of helium into the micropyrolyzer caused the biomass particles to be entrained in the gas flow. The gas flow passed through the three mesh screens in the reactor zone upon which the biomass particles were collected and rapidly heated. Volatiles released from these particles were entrained in the gas flow and passed out of the reactor through the short, deactivated GC column to the FID (see Fig. 2). Although the absence of a conventional GC column prevented speciation of volatile products, the short, deactivated column allowed measurement of the time-resolved response of the FID to the volatile organic compounds. For experiments in which the instrument lag time was significantly shorter than the characteristic time of devolatilization, the FID time-series data could be used to determine global devolatilization rates. We previously developed this technique to study devolatilization of cellulose during pyrolysis [25].

Reactor temperature was varied from 366-600°C in 33°C intervals. Each experiment was repeated a minimum of four times with data recorded at 80 Hz. The screens were replaced after thirty experimental trials to avoid accumulation of ash and char.

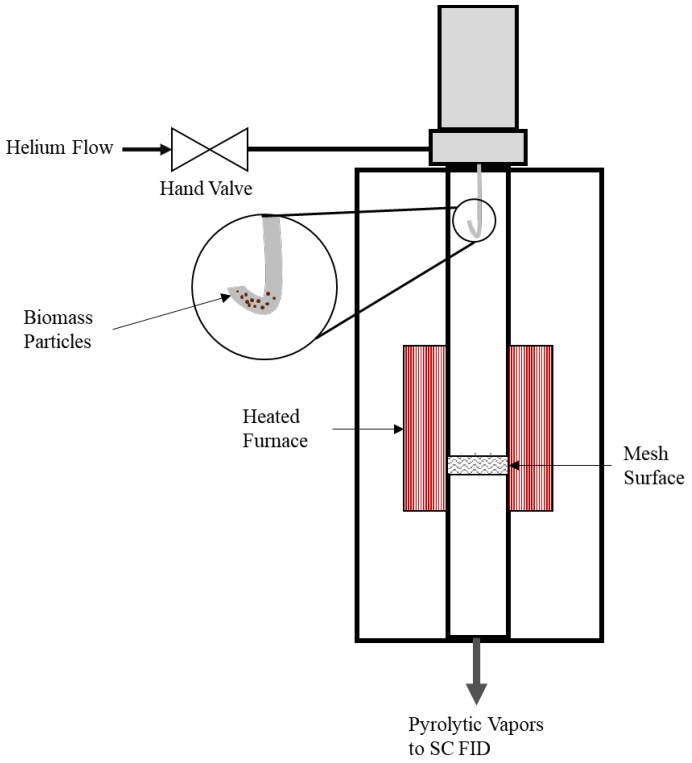

Fig. 1. Micropyrolysis apparatus used to measure devolatilization times of different kinds of biomass. Note: biomass particles are not to scale but enlarged for purposes of illustration.

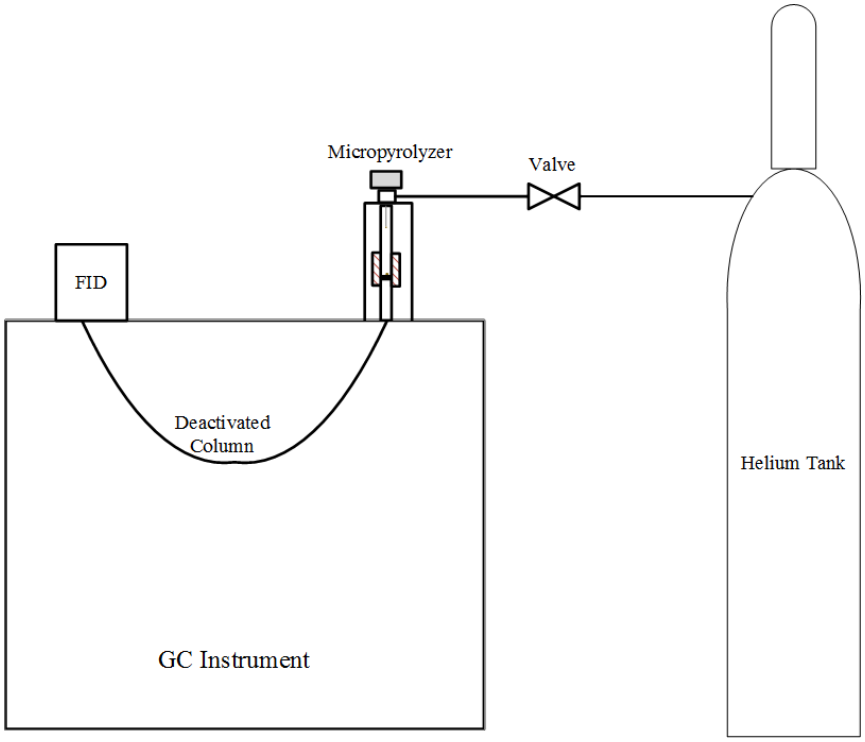

Fig. 2. Schematic of the short column FID set-up used to determine the devolatilization rate.

2.3. Determination of kinetic parameters

FID signals were characterized by a rapid rise followed by a generally more gradual decay. The rise is associated with the lag time of the experimental apparatus while the decay corresponds to the devolatilization. The overall signal to be analyzed was taken to be the point where the FID signal rose to 1% of its eventual maximum level to the point where the FID voltage fell to 3% of the maximum signal. The signal was normalized with respect to the maximum signal from which the extent of reaction, α, was calculated:

$$\alpha(t) = \frac{\theta(t)}{\theta_T} \quad [1]$$

where θ(t) is the integrated FID signal up to time t and θ_T is the integrated FID signal over the total time of reaction. The extend of reaction was fitted to a first order reaction model:

$$\frac{d\alpha}{dt} = \boldsymbol{k}(\mathbf{1} - \boldsymbol{\alpha}) \quad [2]$$

where k is the reaction rate coefficient with units of inverse seconds. A differential equation solver (Python 3: SciPy [34]) was used to determine the reaction rate coefficient from the experimental data.

2.4. Instrument lag determination

Instrument lag time was measured to assure that it was much shorter than devolatilization times, an important requirement for accurately determining devolatilization kinetics. Toward this end, acetone was injected into the micropyrolyzer with furnace temperature held at 600°C. The resulting normalized FID signal is shown in Fig. 3. In the absence of chemical reaction, the

signal rise corresponds to the time for acetone injection time while the slightly longer signal decay corresponds to the instrument lag time.

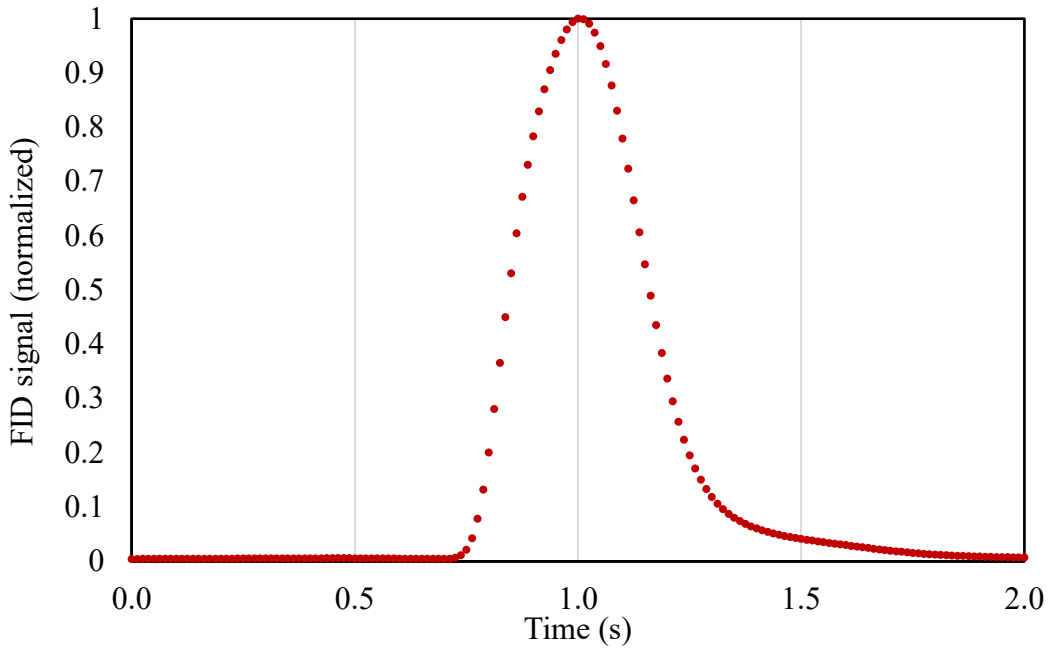

Fig. 3. FID signal from injection of liquid acetone in the apparatus for the purpose of determining instrument lag time from the decay portion of the curve.

The lag time for the experimental apparatus was calculated from the decay portion of the signal and the assumption of continuously stirred tank reactor hydrodynamics [35]:

$$-\ln(S_F) = \tau/t \qquad [3]$$

where S_F is the normalized FID signal, t is the time, and τ is the characteristic lag time. Data was analyzed from the time of peak to where it decayed to 3% of the peak. Accordingly, the characteristic rate of this lag was 6.95 s^{-1}.

2.5. Determination of pyrolysis regime

Meaningful measurement of pyrolysis rates requires that the particles are isothermal and rates are kinetically limited, which requires determination of the pyrolysis regime [36]. Typically,

pyrolysis is characterized by four distinct regimes: convection limited, kinetically limited and isothermal, conduction limited, and kinetically limited and non-isothermal. Three non-dimensional numbers were used to determine these regimes. The first is the Biot number:

$$\mathbf{Bi} = \frac{\mathbf{hD}}{\boldsymbol{\lambda}} \quad [4]$$

where h is the convection coefficient ($Wm^{-2}\,K^{-1}$), D (m) is the characteristic length (particle diameter), and λ (Wm^{-1}-K^{-1}) is the thermal conductivity. The First Pyrolysis Number is a function of the reaction rate (i.e., pyrolysis rate) and the internal heat transfer rate:

$$\mathbf{Py_1} = \frac{\boldsymbol{\lambda}}{\mathbf{kc_pD^2\rho}} \quad [5]$$

where c_p (J kg^{-1}-K^{-1}) is the specific heat of the biomass particle, ρ (kg m^{-3}) is the particle density, and k (s^{-1}) is the reaction rate coefficient. The Second Pyrolysis Number is a function of the external heat transfer rate and the reaction rate:

$$\mathbf{Py_2} = \frac{\mathbf{h}}{\mathbf{kc_pD\rho}} \quad [6]$$

For a kinetically limited and isothermal pyrolysis regime, the Biot number must be less than 1 (preferably 0.1), and the Pyrolysis Numbers greater than 10.

Red oak has a thermal conductivity of 0.15 Wm^{-1}-K^{-1}), specific heat of 1158 J kg^{-1}-K^{-1} (at ambient temperature), and particle density of 650 kg m^{-3}[37]. These values are similar to values reported for other 1-D models, with only slight variation of the parameters (e.g. specific heat and thermal conductivity) between feedstocks [38]. Biomass particle size was estimated to be 60 μm from sieving of biomass samples. The convective heat transfer coefficient was estimated to be 183 $Wm^{-2}\,K^{-1}$ using data reported by Cybulski et. al.[39] for heat transfer at low Reynolds numbers in a packed bed. The radiative contribution to heat transfer rate was estimated to be 42

W/m^2-K resulting in an overall heat transfer rate of 225 $Wm^{-2}\,K^{-1}$. This estimate is comparable to particle-to-wall convection coefficients of 200-320 $Wm^{-2}\,K^{-1}$, reported for heat transfer in fluidized beds [40] [41]. The resulting Biot number is low enough (<0.1) to assume isothermal heat transfer. The First and Second Pyrolysis Numbers were calculated to be 18 and 12820, respectively. These calculations indicate an isothermal pyrolysis regime with kinetically limited reaction [42]. Pyrolysis duration was at least an order of magnitude longer than the heating rate.

3. Results

3.1. Characteristic time constants for devolatilization

The duration of devolatilization was hypothesized to vary by only an order of magnitude in the temperature range of 366-566°C vs two orders of magnitude predicted by the model of Vinu and Broadbelt [21]. This hypothesis is based on previous work in our laboratory in which pyrolysis of red oak quenched after only 0.9 seconds had volatile yields of 15 wt.% and 40 wt.% at reaction temperatures of 400°C and 500°C, respectively [43]. This factor of three increase suggests a relatively low activation energy.

Fig. 4 plots devolatilization rates versus time for several different temperatures. Visual inspection of these results indicates pyrolysis duration decreased from ~20 seconds at 366°C to ~2 second at 500°C respectively. This single order of magnitude difference in duration (366 versus 500°C) indicates a lower activation energy than indicated by the work of Vinu and Broadbelt[21]. Likewise, despite large differences in AAEM content among the feedstocks, the devolatilization rates appear to be similar.

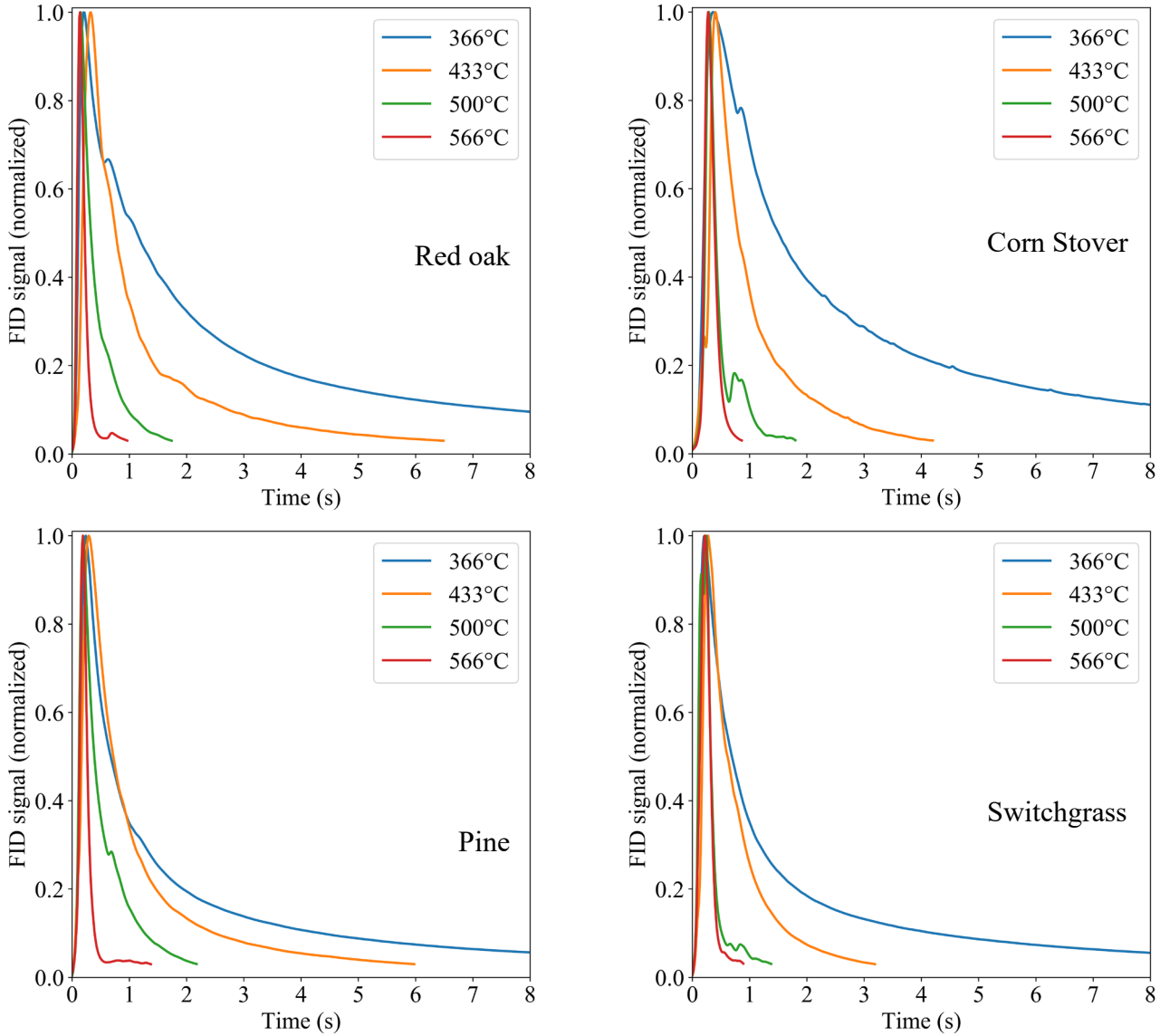

Fig. 4. Normalized FID signal versus reaction time. For visual clarity, the duration for 366°C was only shown to eight seconds, though proceeds until roughly twenty seconds.

0

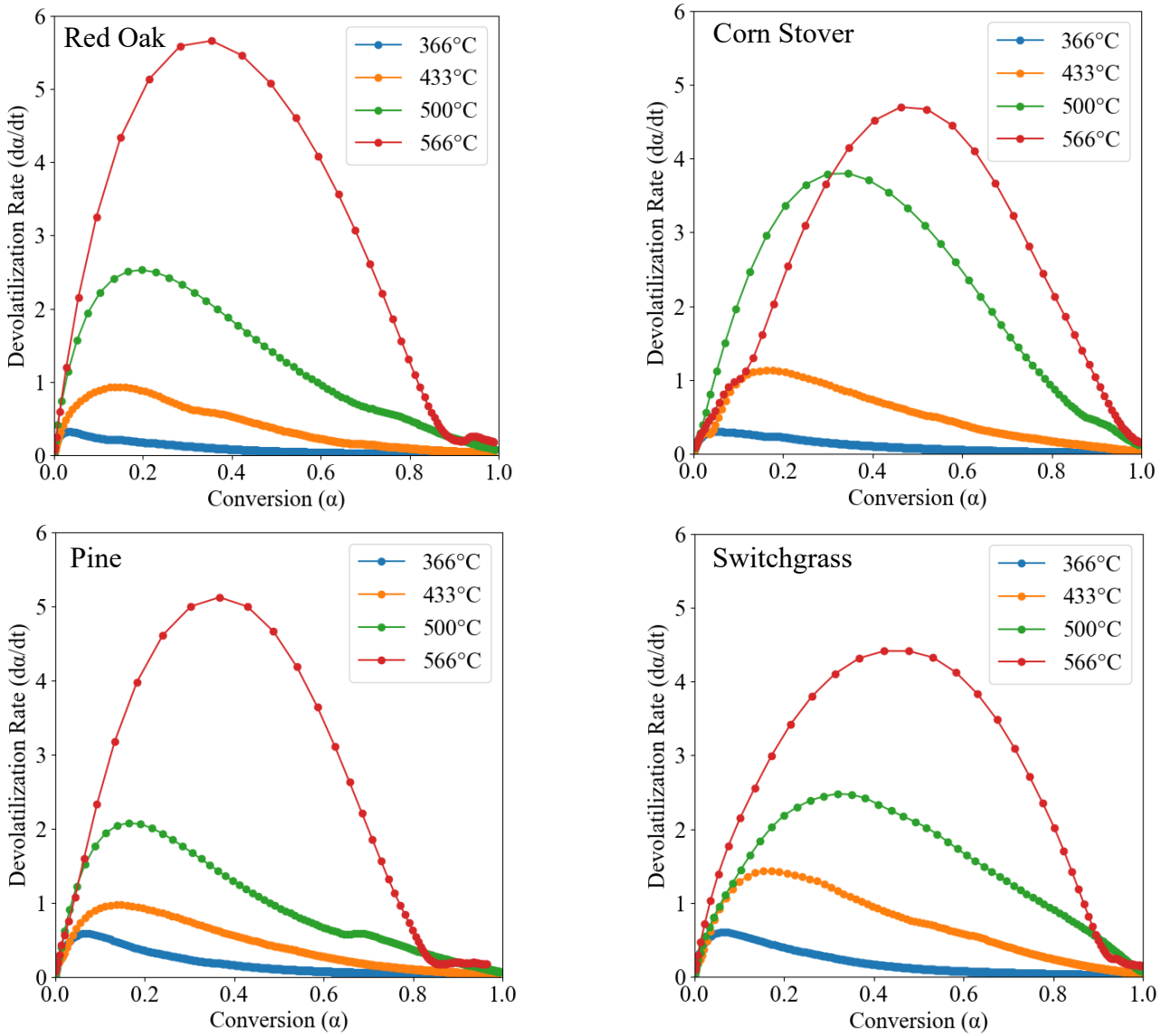

Fig. 5. Devolatilization rate vs conversion for the four biomass samples. The initial rise in devolatilization rate is associated with instrument lag, shifting to the right to higher conversions as temperature increased.

Fig. 5 converts the normalized FID data of Figure 4 into devolatilization rate vs conversion. After the initial rise in rate arising from instrument lag, the rate versus conversion decays in a roughly linear fashion, as expected for the proposed one step model. Accordingly, this data was deemed suitable for calculating kinetic parameters.

Given the proposed one step model, in the absence of instrument lag, the maximum rate occurs near conversion equal to zero. At lower temperatures (e.g., 366°C) the maximum rate is measured at low conversion (<0.05), confirming the single step devolatilization model. In the absence of instrument lag, the maximum rate would occur at zero conversion for a one step model. Thus, when the rate of devolatilization is significantly slower than the instrument lag (e.g. at 366°C) this is true. However, as the temperature is increased, the measured devolatilization rate versus conversion appears parabolic. This shape is not from a two-step model, but from instrument lag distorting the measured apparent rate. Given this instrument lag, all data to the left of the maxima is disregard in the kinetic calculations.

For visual clarity, an additional plot (Fig. 6) was produced for red oak showing the conversion versus the devolatilization rate and the predictions of the one step model. To confirm the accuracy of the one step model, the root mean square error (RMSE) was calculated between the proposed model and the measured data. The average of this RMSE, from the replicate trials at each temperature, and the temperature set-points is shown in Table 4. With the RMSE value being less than 20% of the model and the experimental data (see Table 5 for calculated rate coefficients) the one step model accurately models devolatilization.

Table 4 The calculated root mean square error indicates the one step model well captures biomass devolatilization. Plus and minus value indicates the standard deviation from the replicate trials at each temperature.

	Root Mean Square Error			
Temperature (°C)	**Switchgrass**	**Corn Stover**	**Red Oak**	**Pine**
366	0.05 ±0.01	0.02 ±0.01	0.03 ±0.00	0.05 ±0.00
400	0.08 ±0.02	0.03 ±0.01	0.05 ±0.01	0.06 ±0.01
433	0.07 ±0.01	0.06 ±0.02	0.07 ±0.02	0.08 ±0.00
466	0.11 ±0.06	0.10 ±0.05	0.08 ±0.03	0.08 ±0.01
500	0.18 ±0.14	0.23 ±0.12	0.13 ±0.02	0.10 ±0.01

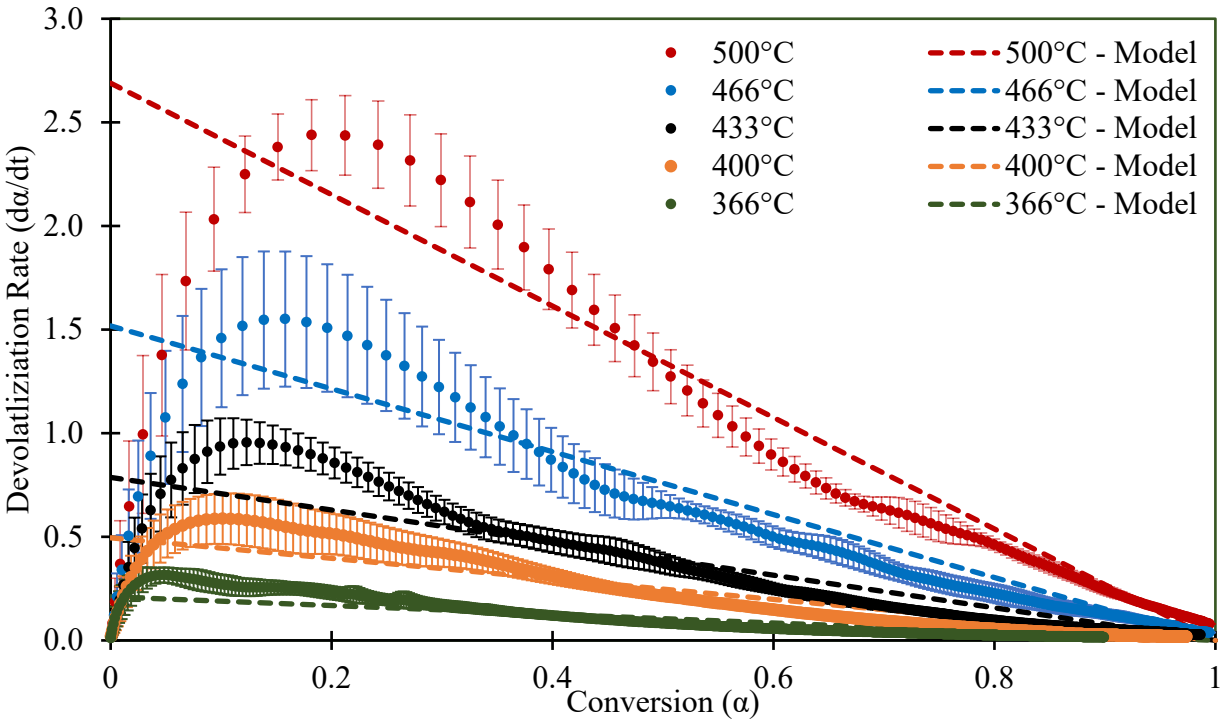

Fig. 6. Devolatilization rate versus conversion was modeled using a one-step model at temperatures below 500°C. Elevated temperatures were not calculated given instrument lag. Error bars represent the sample standard deviation of the rate from the trials (a minimum of four trials were ran at each temperature).

The non-linearity of devolatilization rate versus conversion is thought to reflect differences in decomposition rates of the three kinds of biopolymers in lignocellulosic biomass. At lower heating rates, hemicellulose and cellulose are more reactive than lignin [44]. This effect is commonly seen during TGA studies with the hemicellulose and cellulose portion decomposing at lower temperatures (especially hemicellulose) as compared to lignin [4]. Given the different

decomposition rates under isothermal conditions, the hemicellulose and cellulose biopolymers would have a faster devolatilization rate as compared to the lignin fraction. Thus, it is expected the hemicellulose fraction devolatilizes first [15], with the cellulose and lignin fraction needing additional time to react. These reactivity differences would result in an initial spike in measured rate (above the predicted linear model) as the hemicellulose rapidly devolatilizes, with a longer slower rate associated with the cellulose and lignin fraction devolatilizing. The proposed model could have three individual rates for cellulose, lignin, and hemicellulose; however, the objective of the current study is focused on the overall rate of biomass devolatilization.

Table 5 Devolatilization rate coefficient using a single first order global model. The plus and minus value is the sample standard deviation for each temperature.

	Kinetic Rate Coefficient (s^{-1})			
Temperature (°C)	**Switchgrass**	**Corn Stover**	**Red Oak**	**Pine**
366	0.30 ±0.03	0.19 ±0.02	0.21 ±0.05	0.32 ±0.02
400	0.88 ±0.12	0.55 ±0.07	0.50 ±0.19	0.54 ±0.03
433	1.56 ±0.26	1.17 ±0.28	0.79 ±0.13	0.88 ±0.03
466	2.66 ±0.50	1.70 ±0.24	1.52 ±0.40	1.19 ±0.18
500	4.39 ±0.28*	3.22 ±0.34*	2.69 ±0.24	2.00 ±0.11

*The characteristic times (reciprocal rate coefficients) for switchgrass and corn stover at 500°C are comparable to the instrument lag time thus the reported values likely underestimate the actual rate coefficients. They are not used for subsequent calculation of activation energy.

The devolatilization rate only increased an order of magnitude from 0.19-0.32 s^{-1} to 1.19-2.66 s^{-1} at 366 and 466°C, respectively. This relatively small increase in rate suggests that the apparent activation energy is smaller than measured in previous studies. To determine Arrhenius rate parameters, the logarithm of devolatilization rate coefficients was plotted against the inverse temperature (Fig. 7).

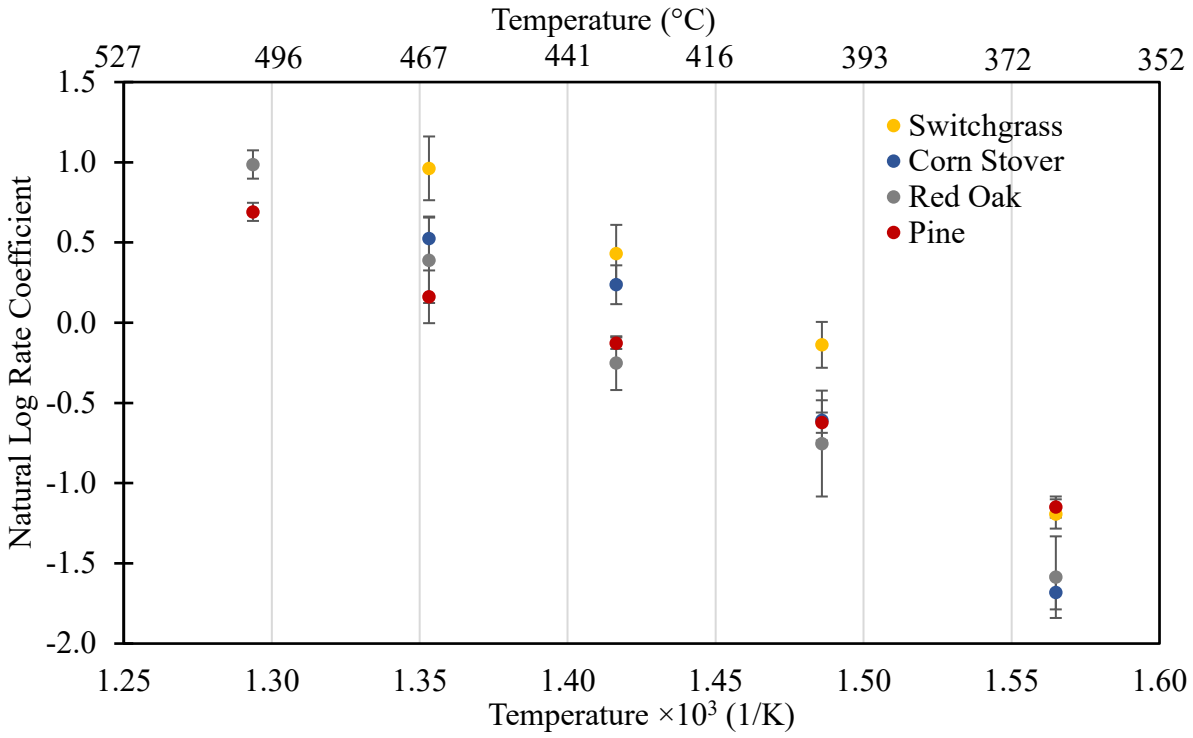

Fig. 7. Arrhenius plot of devolatilization rates. Error bars are the sample standard deviation at each temperature.

The apparent activation energies ranged from 54.9 - 88.4 kJ mol^{-1} for the four biomass feedstocks (Table 6). These apparent activation energies are significantly lower than typically employed in one step devolatilization models. While lower than previous models, Krumm et al.[45] using a rapid heating pyrolyzer measured a similar global activation energy (<77.7 kJ mol^{-1}) for cyclodextrin pyrolysis. Low activation energies have been measured for whole biomass, though experimental conditions are suspect. Van de Velden et al.[46] using TGA studies measured the devolatilization rate of several feedstocks (corn stover, popular, and spruce) calculating activation energies ranging from 54.1-86.4 kJ mol^{-1}. However, as highlighted in the introduction, TGA studies have significantly lower heating rates than fast pyrolysis conditions.

Table 6 Apparent activation and pre-exponential factor from the devolatilization rate. The plus and minus value is the standard deviation of the activation energy. Comparison with other works (using the bio-oil formation rate) indicates these derived values are within previous experimental values.

	Apparent Activation Energy (kJ mol^{-1})	**Pre-Exponential Factor (s^{-1})**	**Calculated Rate Coefficient 400°C (s^{-1})**	**Calculated Rate Coefficient 500°C (s^{-1})**
Switchgrass	83.5 ±4.8	2.24×10^{6}	0.75	5.14
Corn Stover	88.4 ±4.4	3.52×10^{6}	0.49	3.76
Red Oak	77.1 ±4.0	4.20×10^{5}	0.44	2.59
Pine	54.9 ±1.9	9.81×10^{3}	0.53	1.90
Wagenaar et al.[13] (Pine Wood)	150.0	1.40×10^{10}	0.03	1.02
Pielsticker et al.[17] (Beech Wood)	71.3	3.26×10^{4}	0.09	0.49
Zolghadr et al.[20] (Switchgrass)	167.3	2.52×10^{12}	0.26	12.45

These results rectified the inconsistencies of previous models measuring devolatilization kinetics of whole biomass, measuring a relatively low apparent activation energy. Notably, this emphasizes the importance of calculating Biot and Pyrolysis numbers before experimentation, as ignoring these parameters would lead to improperly measured kinetics.

3.2. Effect of biomass composition on devolatilization rate

Alkali and alkaline earth metals (AAEM) are well known to catalyze pyranose ring fragmentation [27]. We hypothesize this catalytic effect will increase the rate of devolatilization. Previous experiments on pyrolysis of cellulose determined potassium has the strongest catalytic effect for cracking pyranose rings, followed by sodium, calcium, and magnesium being the weakest [47]. Studies on char oxidation similarly found potassium to be the strongest catalyst among these metals [48].

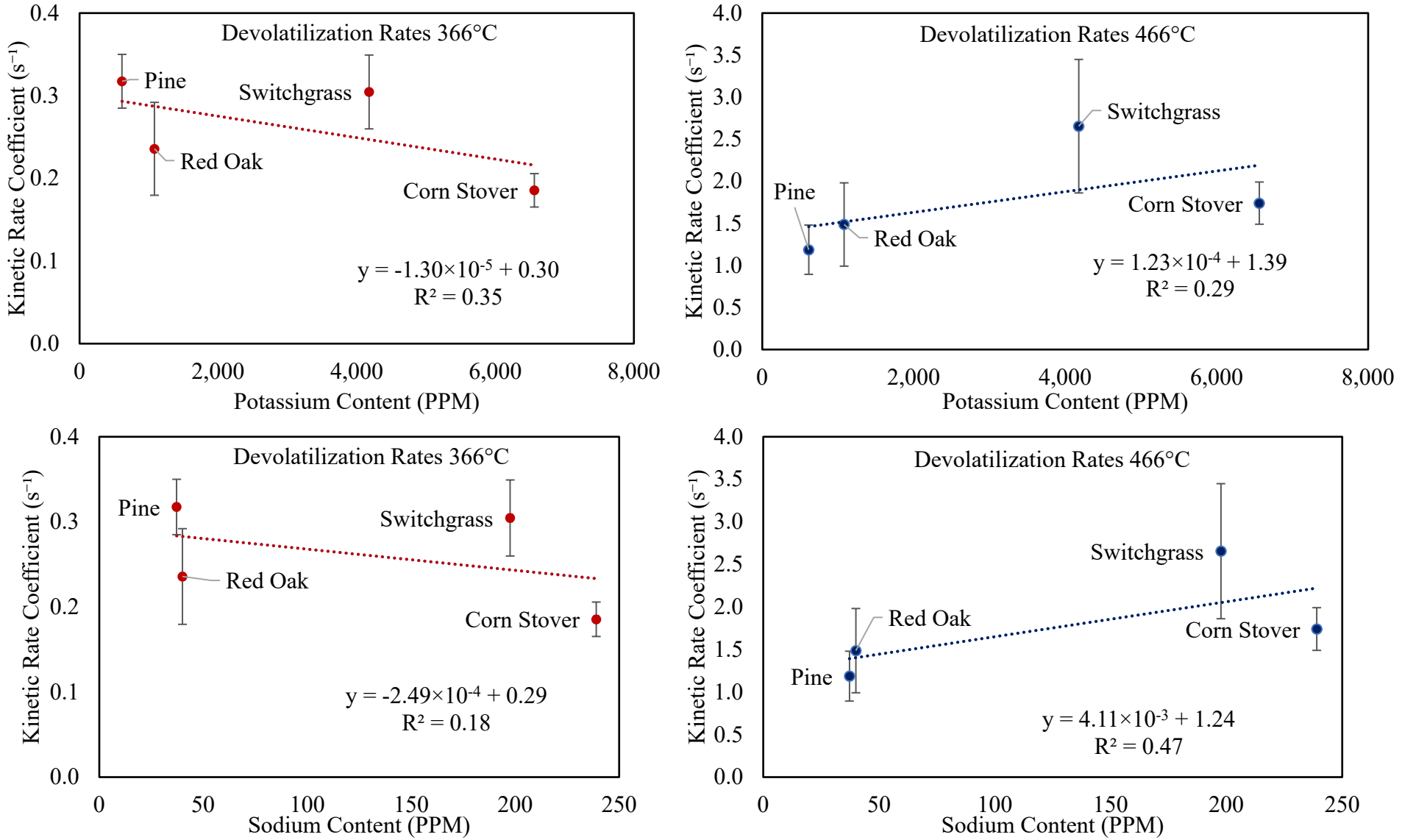

Fig. 8. Simple correlations indicate inorganic content does not affect the devolatilization rate. The low coefficient of determination and inconsistent effect with temperature suggests inorganic content has no effect on the devolatilization rate. Error bars are 95% confidence interval.

Surprisingly, no consistent correlation was observed (Fig. 8) between metal content and devolatilization rate. Likewise, the Student t-test indicates the rates are not statistically significant (p-value 0.05). These results indicate AAEM content does not significantly affect the biomass devolatilization rates.

To confirm AAEM content does not affect the devolatilization rate, corn stover was extensively washed with water to partially remove AAEM content. By washing the feedstock, the original structure and composition remains intact, while removing the water soluble potassium, the most catalytically active of the AAEM content of biomass [49].

Table 7 Calculated devolatilization rate of water-washed corn stover was identical to untreated feedstocks. The plus and minus value is the sample standard deviation.

	Kinetic Rate Coefficient (s^{-1})			
Feedstock	**366°C**	**400°C**	**433°C**	**466°C**
Corn Stover	0.19 ±0.02	0.55 ±0.07	1.17 ±0.28	1.70 ±0.24
Washed Corn Stover	0.21 ±0.01	0.64 ±0.05	0.82 ±0.08	1.40 ±0.25
Significant (α=0.05)	No	No	Yes	No

Performing an identical set of devolatilization experiments (Table 7), the water-washed corn stover did not consistently have statistically significant difference in reaction rate as the unwashed feedstock. This result is similar to the untreated feedstocks, finding no consistent correlation with the reaction rate and metals content.

Johansen et al.[30] made a similar observation for miscanthus, finding after leaching (metals removal) it was within uncertainty of the original rate. Likewise, pine doped with additional KCl had a similar rate to the untreated feedstock (or within uncertainty, again similar to these results). In a similar manner, Branca et al.[50] found that extensive washing of beech wood decreased the initial temperature of cellulose decomposition, as compared to unwashed, though the actual rate

was not calculated. Consequently, these results indicate AAEM content has minimal impact on the devolatilization rate.

4. Conclusions

The devolatilization rates for four kinds of lignocellulosic biomass were determined using a novel micro pyrolyzer. The reactor minimized heat and mass transfer limitations and captured time series data by linking the pyrolyzer to a FID via a short, deactivated GC column. The kinetic data collected in these experiments suggest that activation energies are much smaller than currently assumed in the literature. By carefully controlling experimental parameters, this kinetic data highlights oversights from previous researchers. In particular, calculations must be performed before experimentation to determine the pyrolysis regime and heat transfer rate, ensuring proper kinetic derivation. Experiments with washed feedstocks found that inorganic content did not significantly influence the overall devolatilization rate. This kinetic data will aid in pyrolysis scale-up providing devolatilization kinetics for a variety of feedstocks.

5. Acknowledgements

This work was supported by the Department of Energy under Award Number EE0008326 and DE-AC36-08GO28308. It was prepared as an account of work sponsored by an agency of the United States Government. Neither the United States Government nor any agency thereof, nor any of their employees, makes any warranty, express or implied, or assumes any legal liability or responsibility for the accuracy, completeness, or usefulness of any information, apparatus, product, or process disclosed, or represents that its use would not infringe privately owned rights. Reference herein to any specific commercial product, process, or service by trade name, trademark, manufacturer, or otherwise does not necessarily constitute or imply its endorsement,

recommendation, or favoring by the United States Government or any agency thereof. The views and opinions of authors expressed herein do not necessarily state or reflect those of the United States Government or any agency thereof.

The authors would like to thank Jake Lindstrom, Sean Rollag, and Ryan Smith of the Bioeconomy Institute for insightful discussions. The authors also want to thank Jessica Brown of the Bioeconomy Institute for providing key and critical valuable information on the particle sizes. The authors would also like to thank John Peterson of Northern State University for providing insight on the statistical methods.

6. CRediT authorship contribution statement

Chad Peterson: Data curation, Methodology, Writing -Original Draft, Investigation. **Malachi Hornbuckle**: Writing -Review and Editing, Methodology, Investigation. **Robert Brown:** Writing -Review and Editing, Supervision, Project administration, Funding acquisition.

References

[1] R.C. Brown, Thermochemical Processing of Biomass: Conversion into Fuels, Chemicals and Power, John Wiley & Sons, Ltd, Chichester, UK, 2011. https://doi.org/10.1002/9781119990840.

[2] C. Di Blasi, Modeling chemical and physical processes of wood and biomass pyrolysis, Prog. Energy Combust. Sci. 34 (2008) 47–90. https://doi.org/10.1016/j.pecs.2006.12.001.

[3] M.B. Pecha, J.I.M. Arbelaez, M. Garcia-Perez, F. Chejne, P.N. Ciesielski, Progress in understanding the four dominant intra-particle phenomena of lignocellulose pyrolysis: chemical reactions, heat transfer, mass transfer, and phase change, Green Chem. (2019). https://doi.org/10.1039/C9GC00585D.

[4] R.S. Miller, J. Bellan, A generalized biomass pyrolysis model based on superimposed cellulose, hemicellulose and lignin kinetics, Combust. Sci. Technol. 126 (1997) 97–137. https://doi.org/10.1080/00102209708935670.

[5] C. Di Blasi, Numerical simulation of cellulose pyrolysis, Biomass and Bioenergy. 7 (1994) 87–98. https://doi.org/10.1016/0961-9534(94)00040-Z.

[6] A.G.W. Bradbury, Y. Sakai, F. Shafizadeh, A kinetic model for pyrolysis of cellulose, J. Appl. Polym. Sci. 23 (1979) 3271–3280. https://doi.org/10.1002/app.1979.070231112.

[7] C. Di Blasi, C. Branca, C.D.B. and, C. Branca, C. Di Blasi, C. Branca, Kinetics of Primary Product Formation from Wood Pyrolysis, Ind. Eng. Chem. Res. 40 (2002) 5547–5556. https://doi.org/10.1021/ie000997e.
[8] J.K. Lindstrom, A. Shaw, X. Zhang, R.C. Brown, Condensed Phase Reactions During Thermal Deconstruction, in: Thermochem. Process. Biomass, John Wiley & Sons, Ltd, Chichester, UK, 2019: pp. 17–48. https://doi.org/10.1002/9781119417637.ch2.
[9] M.S. Safdari, E. Amini, D.R. Weise, T.H. Fletcher, Heating rate and temperature effects on pyrolysis products from live wildland fuels, Fuel. 242 (2019) 295–304. https://doi.org/10.1016/j.fuel.2019.01.040.
[10] P. Ranganathan, S. Gu, Computational fluid dynamics modelling of biomass fast pyrolysis in fluidised bed reactors, focusing different kinetic schemes, Bioresour. Technol. 213 (2016) 333–341. https://doi.org/10.1016/j.biortech.2016.02.042.
[11] J. Matta, B. Bronson, P.E.G. Gogolek, D. Mazerolle, J. Thibault, P. Mehrani, Comparison of multi-component kinetic relations on bubbling fluidized-bed woody biomass fast pyrolysis reactor model performance, Fuel. 210 (2017) 625–638. https://doi.org/10.1016/j.fuel.2017.08.092.
[12] A.K. Sadhukhan, P. Gupta, R.K. Saha, Modelling and experimental studies on pyrolysis of biomass particles, J. Anal. Appl. Pyrolysis. 81 (2008) 183–192. https://doi.org/10.1016/j.jaap.2007.11.007.
[13] B.M. Wagenaar, W. Prins, W.P.M. van Swaaij, Flash pyrolysis kinetics of pine wood, Fuel Process. Technol. 36 (1993) 291–298. https://doi.org/10.1016/0378-3820(93)90039-7.
[14] A.M.C. Janse, R.W.J. Westerhout, W. Prins, Modelling of flash pyrolysis of a single wood particle, Chem. Eng. Process. Process Intensif. 39 (2000) 239–252. https://doi.org/10.1016/S0255-2701(99)00092-6.
[15] P. Gable, R.C. Brown, Effect of biomass heating time on bio-oil yields in a free fall fast pyrolysis reactor, Fuel. 166 (2016) 361–366. https://doi.org/10.1016/J.FUEL.2015.10.073.
[16] A.G. Liden, F. Berruti, D.S. Scott, A kinetic model for the production of liquids from the flash pyrolysis of biomass, Chem. Eng. Commun. 65 (1988) 207–221. https://doi.org/10.1080/00986448808940254.
[17] S. Pielsticker, K. Schlögel, T. Kreitzberg, O. Hatzfeld, R. Kneer, Biomass pyrolysis kinetics in a fluidized bed reactor: Measurements and plausibility verification for reaction conditions, Fuel. 254 (2019) 115589. https://doi.org/10.1016/j.fuel.2019.05.172.
[18] A.D. Paulsen, M.S. Mettler, P.J. Dauenhauer, The role of sample dimension and temperature in cellulose pyrolysis, Energy and Fuels. 27 (2013) 2126–2134. https://doi.org/10.1021/ef302117j.
[19] A. Zolghadr, J.J. Biernacki, R.J. Moore, Biomass Fast Pyrolysis Using a Novel Microparticle Microreactor Approach: Effect of Particles Size, Biomass Type, and Temperature, Energy & Fuels. 33 (2018) 1146–1156. https://doi.org/10.1021/ACS.ENERGYFUELS.8B03395.
[20] A. Zolghadr, C. Templeton, J.J. Biernacki, Biomass Fast Pyrolysis Using a Novel Microsphere Microreactor Approach: Model-Based Interpretations, Energy and Fuels. 33 (2019) 10999–11008. https://doi.org/10.1021/acs.energyfuels.9b02209.
[21] R. Vinu, L.J. Broadbelt, A mechanistic model of fast pyrolysis of glucose-based carbohydrates to predict bio-oil composition, Energy Environ. Sci. 5 (2012) 9808–9826. https://doi.org/10.1039/c2ee22784c.

[22] X. Zhou, W. Li, R. Mabon, L.J. Broadbelt, A mechanistic model of fast pyrolysis of hemicellulose, Energy Environ. Sci. 11 (2018) 1240–1260. https://doi.org/10.1039/C7EE03208K.
[23] R.H. Venderbosch, Fast Pyrolysis, in: Thermochem. Process. Biomass, John Wiley & Sons, Ltd, Chichester, UK, 2019: pp. 175–206. https://doi.org/10.1002/9781119417637.ch6.
[24] A.K. Burnham, X. Zhou, L.J. Broadbelt, Critical Review of the Global Chemical Kinetics of Cellulose Thermal Decomposition, Energy & Fuels. 29 (2015) 2906–2918. https://doi.org/10.1021/acs.energyfuels.5b00350.
[25] J.K. Lindstrom, J. Proano-Aviles, P.A. Johnston, C.A. Peterson, J.S. Stansell, R.C. Brown, Competing reactions limit levoglucosan yield during fast pyrolysis of cellulose, Green Chem. 21 (2019) 178–186. https://doi.org/10.1039/c8gc03461c.
[26] S.A. Rollag, J.K. Lindstrom, R.C. Brown, Pretreatments for the continuous production of pyrolytic sugar from lignocellulosic biomass, Chem. Eng. J. 385 (2020) 123889. https://doi.org/10.1016/j.cej.2019.123889.
[27] N. Kuzhiyil, D. Dalluge, X. Bai, K.H. Kim, R.C. Brown, Pyrolytic Sugars from Cellulosic Biomass, ChemSusChem. 5 (2012) 2228–2236. https://doi.org/10.1002/cssc.201200341.
[28] A. Saddawi, J.M. Jones, A. Williams, Influence of alkali metals on the kinetics of the thermal decomposition of biomass, Fuel Process. Technol. 104 (2012) 189–197. https://doi.org/10.1016/J.FUPROC.2012.05.014.
[29] D. Zhao, Y. Dai, K. Chen, Y. Sun, F. Yang, K. Chen, Effect of potassium inorganic and organic salts on the pyrolysis kinetics of cigarette paper, J. Anal. Appl. Pyrolysis. 102 (2013) 114–123. https://doi.org/https://doi.org/10.1016/j.jaap.2013.03.007.
[30] J.M. Johansen, P.A. Jensen, P. Glarborg, N. De Martini, P. Ek, R.E. Mitchell, High Heating Rate Devolatilization Kinetics of Pulverized Biomass Fuels, Energy and Fuels. 32 (2018) 12955–12961. https://doi.org/10.1021/acs.energyfuels.8b03100.
[31] H.B. Mayes, M.W. Nolte, G.T. Beckham, B.H. Shanks, L.J. Broadbelt, The Alpha-Bet(a) of Salty Glucose Pyrolysis: Computational Investigations Reveal Carbohydrate Pyrolysis Catalytic Action by Sodium Ions, in: ACS Catal., 2015: pp. 192–202. https://doi.org/10.1021/cs501125n.
[32] J.P. Polin, C.A. Peterson, L.E. Whitmer, R.G. Smith, R.C. Brown, Process intensification of biomass fast pyrolysis through autothermal operation of a fluidized bed reactor, Appl. Energy. 249 (2019) 276–285. https://doi.org/10.1016/J.APENERGY.2019.04.154.
[33] J.P. Polin, H.D. Carr, L.E. Whitmer, R.G. Smith, R.C. Brown, Conventional and autothermal pyrolysis of corn stover: Overcoming the processing challenges of high-ash agricultural residues, J. Anal. Appl. Pyrolysis. 143 (2019) 104679. https://doi.org/10.1016/j.jaap.2019.104679.
[34] P. Virtanen, R. Gommers, T.E. Oliphant, M. Haberland, T. Reddy, D. Cournapeau, E. Burovski, P. Peterson, W. Weckesser, J. Bright, S.J. van der Walt, M. Brett, J. Wilson, K.J. Millman, N. Mayorov, A.R.J. Nelson, E. Jones, R. Kern, E. Larson, C.J. Carey, İ. Polat, Y. Feng, E.W. Moore, J. VanderPlas, D. Laxalde, J. Perktold, R. Cimrman, I. Henriksen, E.A. Quintero, C.R. Harris, A.M. Archibald, A.H. Ribeiro, F. Pedregosa, P. van Mulbregt, A. Vijaykumar, A. Pietro Bardelli, A. Rothberg, A. Hilboll, A. Kloeckner, A. Scopatz, A. Lee, A. Rokem, C.N. Woods, C. Fulton, C. Masson, C. Häggström, C. Fitzgerald, D.A. Nicholson, D.R. Hagen, D. V. Pasechnik, E. Olivetti, E. Martin, E. Wieser, F. Silva, F. Lenders, F. Wilhelm, G. Young, G.A. Price, G.L. Ingold, G.E. Allen,

G.R. Lee, H. Audren, I. Probst, J.P. Dietrich, J. Silterra, J.T. Webber, J. Slavič, J. Nothman, J. Buchner, J. Kulick, J.L. Schönberger, J.V. de Miranda Cardoso, J. Reimer, J. Harrington, J.L.C. Rodríguez, J. Nunez-Iglesias, J. Kuczynski, K. Tritz, M. Thoma, M. Newville, M. Kümmerer, M. Bolingbroke, M. Tartre, M. Pak, N.J. Smith, N. Nowaczyk, N. Shebanov, O. Pavlyk, P.A. Brodtkorb, P. Lee, R.T. McGibbon, R. Feldbauer, S. Lewis, S. Tygier, S. Sievert, S. Vigna, S. Peterson, S. More, T. Pudlik, T. Oshima, T.J. Pingel, T.P. Robitaille, T. Spura, T.R. Jones, T. Cera, T. Leslie, T. Zito, T. Krauss, U. Upadhyay, Y.O. Halchenko, Y. Vázquez-Baeza, SciPy 1.0: fundamental algorithms for scientific computing in Python, Nat. Methods. 17 (2020) 261–272. https://doi.org/10.1038/s41592-019-0686-2.

[35] N.J. Christofides, R.C. Brown, Coal burning properties determined from CO2 profiles, Combust. Flame. 94 (1993) 449–461. https://doi.org/10.1016/0010-2180(93)90126-N.

[36] D.L. Pyle, C.A. Zaror, Heat transfer and kinetics in the low temperature pyrolysis of solids, Chem. Eng. Sci. 39 (1984) 147–158. https://doi.org/10.1016/0009-2509(84)80140-2.

[37] S. V. Glass, S.L. Zelinka, Wood Handbook, Chapter 04: Moisture Relations and Physical Properties of Wood, Department of Agriculture, Forest Service, Forest Products Laboratory, Madison, WI: U.S., WI: U.S., 2010.

[38] G.M. Wiggins, P.N. Ciesielski, C.S. Daw, Low-Order Modeling of Internal Heat Transfer in Biomass Particle Pyrolysis, Energy and Fuels. 30 (2016) 4960–4969. https://doi.org/10.1021/acs.energyfuels.6b00554.

[39] A. Cybulski, M.J. Van Dalen, J.W. Verkerk, P.J. Van Den Berg, Gas-particle heat transfer coefficients in packed beds at low Reynolds numbers, Chem. Eng. Sci. 30 (1975) 1015–1018. https://doi.org/10.1016/0009-2509(75)87002-3.

[40] P. Mellin, E. Kantarelis, W. Yang, Computational fluid dynamics modeling of biomass fast pyrolysis in a fluidized bed reactor, using a comprehensive chemistry scheme, Fuel. 117 (2014) 704–715. https://doi.org/10.1016/j.fuel.2013.09.009.

[41] K. Papadikis, S. Gu, A. V. Bridgwater, CFD modelling of the fast pyrolysis of biomass in fluidised bed reactors: Modelling the impact of biomass shrinkage, Chem. Eng. J. 149 (2009) 417–427. https://doi.org/10.1016/j.cej.2009.01.036.

[42] G. SriBala, H.H. Carstensen, K.M. Van Geem, G.B. Marin, Measuring biomass fast pyrolysis kinetics: State of the art, 2019. https://doi.org/10.1002/wene.326.

[43] J.K. Lindstrom, Analyzing and exploiting biomass thermal deconstruction, Iowa State University, 2019. https://lib.dr.iastate.edu/etd/17242.

[44] J.Y. Yeo, B.L.F. Chin, J.K. Tan, Y.S. Loh, Comparative studies on the pyrolysis of cellulose, hemicellulose, and lignin based on combined kinetics, J. Energy Inst. 92 (2019) 27–37. https://doi.org/10.1016/j.joei.2017.12.003.

[45] C. Krumm, J. Pfaendtner, P.J. Dauenhauer, Millisecond Pulsed Films Unify the Mechanisms of Cellulose Fragmentation, Chem. Mater. 28 (2016) 3108–3114. https://doi.org/10.1021/acs.chemmater.6b00580.

[46] M. Van de Velden, J. Baeyens, A. Brems, B. Janssens, R. Dewil, Fundamentals, kinetics and endothermicity of the biomass pyrolysis reaction, Renew. Energy. 35 (2010) 232–242. https://doi.org/10.1016/j.renene.2009.04.019.

[47] P.R. Patwardhan, J.A. Satrio, R.C. Brown, B.H. Shanks, Influence of inorganic salts on the primary pyrolysis products of cellulose, Bioresour. Technol. 101 (2010) 4646–4655. https://doi.org/10.1016/j.biortech.2010.01.112.

[48] C.A. Peterson, R.C. Brown, Oxidation kinetics of biochar from woody and herbaceous biomass, Chem. Eng. J. 401 (2020) 126043. https://doi.org/10.1016/j.cej.2020.126043.
[49] L. Deng, T. Zhang, D. Che, Effect of water washing on fuel properties, pyrolysis and combustion characteristics, and ash fusibility of biomass, Fuel Process. Technol. 106 (2013) 712–720. https://doi.org/10.1016/j.fuproc.2012.10.006.
[50] C. Branca, A. Albano, C. Di Blasi, Critical evaluation of global mechanisms of wood devolatilization, Thermochim. Acta. 429 (2005) 133–141. https://doi.org/10.1016/j.tca.2005.02.030.